

GLOBAL JOURNAL OF ENGINEERING SCIENCE AND RESEARCHES POST DEPOSITION TEMPERATURE-DEPENDENT OPTICAL AND SOLID STATE PROPERTIES OF CHEMICALLY DEPOSITED ZNS/FE₂O₃ CORE-SHELL THIN FILMS

Richard .O. Okoro^{1,2*}, Mishark .N. Nnabuchi¹, & Chukwuemeka Augustine³

¹Department of Industrial Physics, Ebonyi State University, Abakaliki, Nigeria

²Department of Physics, Ebonyi State College of Education, Ebonyi State, Nigeria

³Department of Physics/Geology/Geophysics, Alex Ekwueme Federal University Ndufu-Alike
Ikwo, Ebonyi State, Nigeria

Abstract

ZnS/Fe₂O₃ core-shell thin films were deposited on glass substrates via the chemical bath deposition technique. The films were subsequently annealed in ambient air between 150°C and 200°C. The elemental components of Zn, S, Fe and O were quantitatively obtained from RBS analysis, confirming the formation of ZnS/Fe₂O₃ core-shell thin films. The scanning electron microscopy studies indicated homogeneity of particle distribution with increase in post deposition temperature. The optical properties of the films were characterized by UV-Vis spectroscopy in the wavelength range 300-1000nm. The result of optical characterization showed that absorbance vary from 0.05-0.45, 0.05-0.52 and 0.12-0.70 for as-grown, annealed at 150°C and 200°C respectively. The transmittance generally vary from 35-93%, 30-93% and 20-88% for as-grown, annealed at 150°C and 200°C samples respectively. The energy band gap exhibited red shift, decreasing from 3.90eV to 3.85eV. The extinction coefficient, refractive index, real and imaginary parts of dielectric constant varied accordingly with post deposition temperature. Based on the property of high transmittance in the visible region and wide band gap exhibited by the films, it can be concluded that the films are suitable materials for photovoltaic applications.

Keywords: Band gap, photovoltaic, chemical bath, annealing, core-shell.

I. INTRODUCTION

Zinc sulphide is a wide band gap semiconductor and as such has found much use in solar cells as a window layer for narrow band gap materials such as lead sulphide. Zinc sulphide is widely used as the base materials for cathode-ray tube luminescent materials, catalysts, electroluminescent devices, and UV semiconductor lasers for optical lithography [1]. ZnS is an important II–VI compound semiconductor, crystallising in two phases, cubic-type zinc blende and hexagonal-type wurtzite, with band gaps of 3.66eV and 3.74eV respectively [2]. Fe₂O₃ is the most stable oxide of iron and is environmentally friendly (non-toxic), highly resistant to corrosion and ferromagnetic [3]. It occurs naturally in the form of a mineral resource called hematite which is the major source of iron used in producing steel [4]. In the form of fine powder, α -Fe₂O₃ is used in polishing metallic jewelry and lenses [5]. Alpha-Fe₂O₃ is used as catalyst for petrochemical applications [6] and also has biomedical applications [7,8].

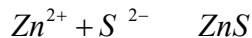
Currently, there is an increasing emphasis on the synthesis of core-shell thin films due to the fascinating synergetic properties or complimentary behaviours offered by the composite nanostructures. The survey of literature showed that core-shell thin films have been deposited using both physical and chemical methods. The physical methods include thermal evaporation [9], sputtering [10] and epitaxial technique [11] while the chemical methods include chemical bath deposition [12-17], spray pyrolysis [18], sol-gel [19, 20], chemical vapour deposition [21] etc. In this work, we report the chemical bath deposition of ZnS/Fe₂O₃ core-shell thin films, with emphasis on the effect of post deposition temperature on the of the optical and solid state properties of the grown films.

II. MATERIALS AND METHODS

First, ZnS films was deposited using a bath composition of 2-8mls of 0.2M of ZnCl₂, 6 mls of 0.2 (NH₂)₂CS, 7mls of 10M NH₃ solution at 60°C. The deposition of ZnS/Fe₂O₃ core-shell thin films was achieved by inserting the glass substrates covered with ZnS films into a chemical bath containing 10mls, 0.5M of FeSO₄.7H₂O, 10mls of 0.5M of KCl, 2 drops of 1M of NaOH (complexing agent) and 38mls of distilled water in that order with P^H between 3.6 at 60°C bath temperature for 2 hours. Thermo scientific GENESYS 10S model UV-VIS spectrophotometer was used to determine the transmittance of the films in the wavelength range of 300-1000 nm at Centre for Energy Research and Development (CERD), OAU, Ile-Lfe, Osun State. The chemical reactions involved in the deposition of ZnS thin films are as follows [22].



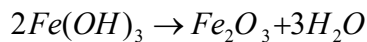
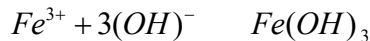
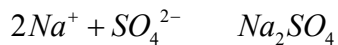
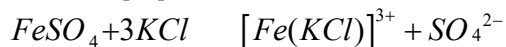
In the above reaction, a zinc complex called zinc diamine chloride $[Zn(NH_3)_2]Cl_2$ is formed which slowly releases the zinc ions in the solution as follows:



Taken together, the total reaction becomes:



The step wise ionic reaction involved in the complex ion formation and film deposition processes for Fe₂O₃ films are as follows [23].



III. RESULT AND DISCUSSION

Fig.1 depicts the RBS micrograph of ZnS/Fe₂O₃ core-shell thin film. A glance on the figure indicated that all the elements that make up the core-shell are present. The quantitative measurement of the elemental composition showed that Zn (1.98%), S (46.92%), O (51.10%) , and Fe (1.97%) confirming the formation of ZnS/Fe₂O₃ core-shell thin films. The glass substrates composed of Si (34.0%), O (26.0%), Ca (6.0%), Na (25.0%), Al (5.2%), K(3.50%) and Fe (0.30%).

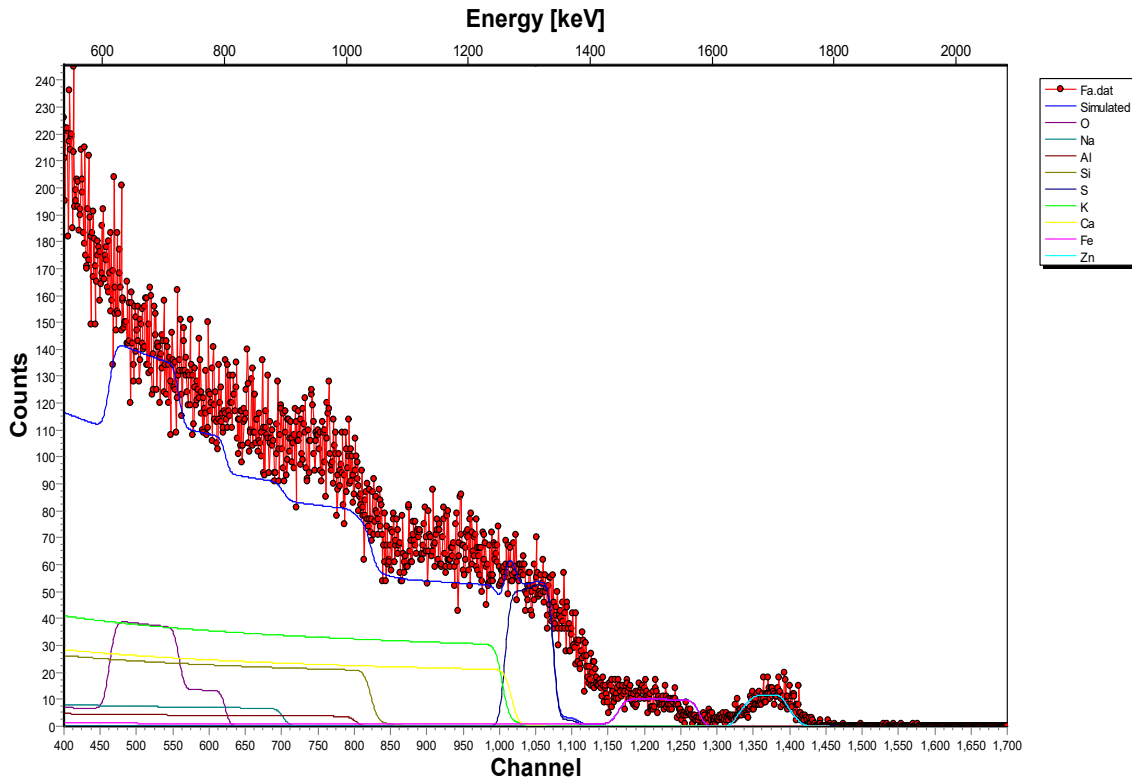


Fig.1: RBS micrograph of ZnS/Fe₂O₃ core-shell thin films

The SEM micrographs for as-grown, annealed at 150°C and 200°C are shown in Figures 2, 3 and 4 respectively.

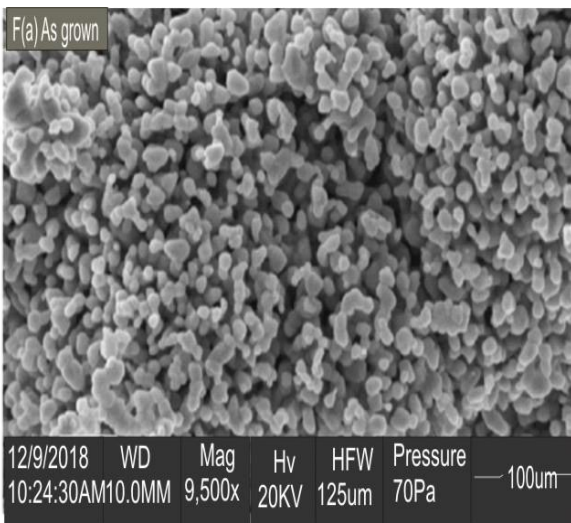


Fig.2: SEM micrograph for as-grown sample

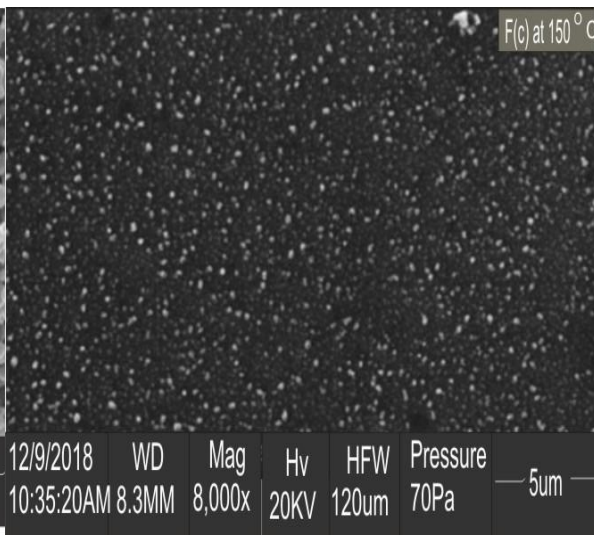


Fig.3: SEM micrograph for annealed at 150°C

A close observation of the scanning electron micrographs of ZnS/Fe₂O₃ core-shell thin films show that homogeneity of the grain size increased with post deposition temperature. Engagement of small grains of the films in flower-like

structure is clearly observed in SEM micrograph of the films, suggesting nano-structured films. The observed long network structure ordering makes the films good material for design of light-trapping configuration for solar cells [24].

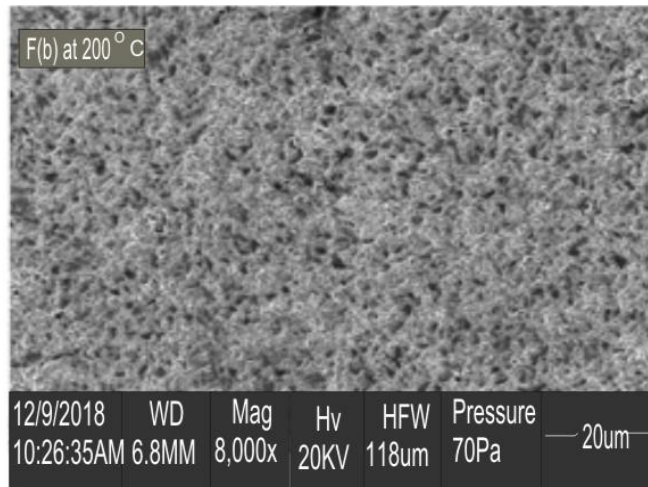


Fig.4: SEM micrograph for annealed at 200°C

The plot of absorbance against wavelength is shown in fig.5. The absorbance increased with post deposition temperature. The absorbance vary from 0.05-0.45, 0.05-0.52 and 0.12-0.70 for as-grown, annealed at 150°C and 200°C respectively. The absorbance generally decreased with wavelength exhibiting a minimum in the infrared region. Enhanced absorption is observed in the neighbourhood of 300-400nm. Our range of absorbance is lower compared to that of Agbo and Nnabuchi (2011) for TiO₂/Fe₂O₃ core-shell thin film [25], Augustine and Nnabuchi (2018) for CuO/PbS double layer thin films [14] and Augustine et al (2017) for PbS/NiO core-shell thin films [12]. The lower absorbance may be associated with the concentration of the reagents used. It is reported in the literature that dilute solutions have absorbance ≤ 2 in accordance with Lambert-Beer's law [26]. Accordingly, the absorbance of ZnS/Fe₂O₃ core-shell thin films at different post deposition temperature satisfied the Lambert-Beer equation.

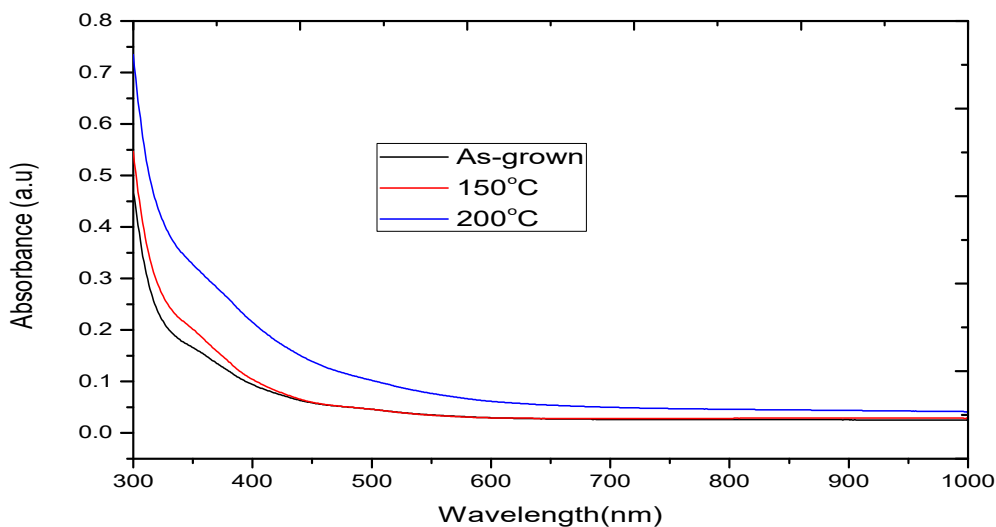


Fig.5: Plot of absorbance against wavelength

The plots of transmittance against wavelength at different post deposition temperature is shown in Fig.6. The transmittance spectra indicates that the transmittance increased with wavelength exhibiting a minimum for film sample annealed at 200°C. The transmittance generally vary from 35-93%, 30-93% and 20-88% for as-grown, annealed at 150°C and 200°C samples respectively. The overall decrease in the transmittance of the films with increase in post deposition temperature may be associated with the increase in particle size. The transmittance of ZnS/Fe₂O₃ films is in general above 50% in the visible region of solar spectrum. Human eye is sensitive only to the range 400-700nm and is peaked at 500nm [27]. This is an important factor in window coatings and is met in these films. The high transmittance of the films in the infrared region placed them as suitable materials for construction of roofs and walls of poultry houses. This will facilitate transmission of infrared radiation (thermal portion of electromagnetic spectrum) into the building for warming young chicks and has the potential to reduce the cost of energy consumption associated with the use of electric bulbs, stoves and lambs to generate heat. These findings are in agreement with that of Augustine and Nnabuchi (2018) for CuO/PbS thin films [14], Kalu et al (2018) for CeO thin films [28], Chikwenze and Ekpunobi (2007) for PbSe thin films [29].

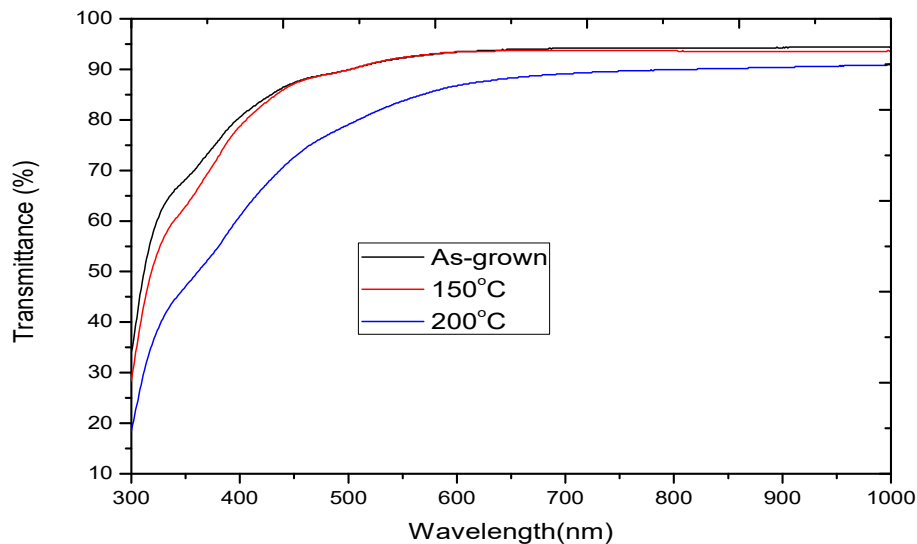


Fig.6: Plot of Transmittance against wavelength

The details of the mathematical determination of the absorption coefficient (α) can be found in literature [30, 31] while the plots of absorption coefficient against photon energy is shown in fig.7. These absorption spectra, which are the most direct and perhaps the simplest method for probing the band structure of semiconductors, are employed in the determination of the energy gap, E_g . The optical band gap E_g was calculated using Tauc's plot $(\alpha h\nu)^2$ versus $h\nu$ [32, 33] as shown in fig.8. The value of α is determined from transmittance spectra. The photon energy at the point where $(\alpha h\nu)^2$ is zero represents E_g , which is determined by extrapolation. The obtained direct band gap are 3.90eV, 3.88eV and 3.85eV for as-deposited, annealed at 150°C and 200°C respectively. Accordingly, the blue exhibit a red shift i.e decreased with annealing temperature. It is believed that thin films whose band gap values decrease with annealing temperature has particle distribution which increases with thermal annealing. The decrease in the energy band gap is possibly due to the decrease in the number of defects, evaporation of water molecules off the films and reorganization of the films. The temperature dependence parameters that affect the band gap are reorganization of the film and self-oxidation [34]. The reorganization of the film should occur at all annealing temperature. By filling the voids in the film one expects denser films and lower energy gaps [29].

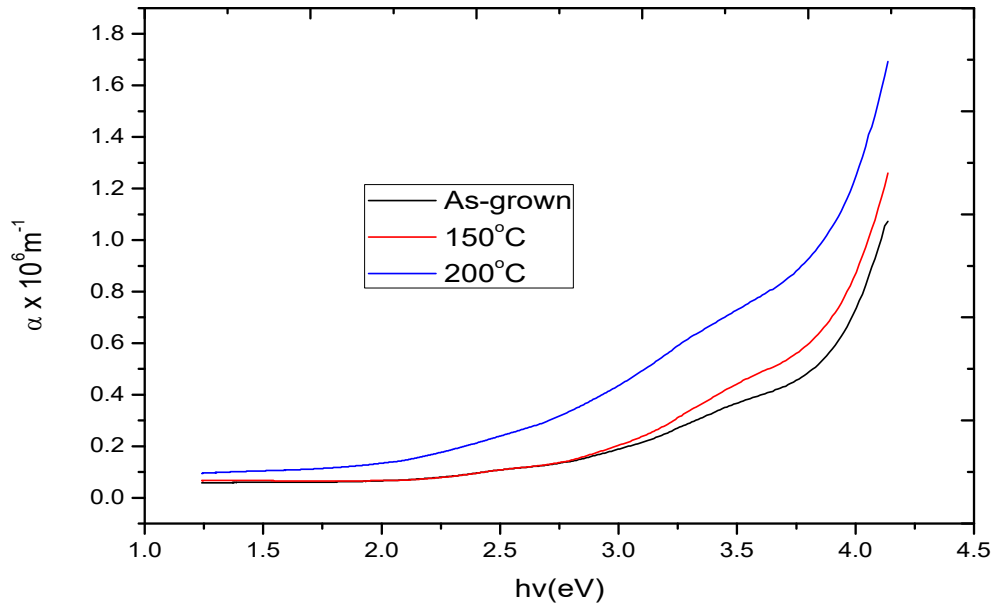


Fig.7: Plots of α versus photon energy

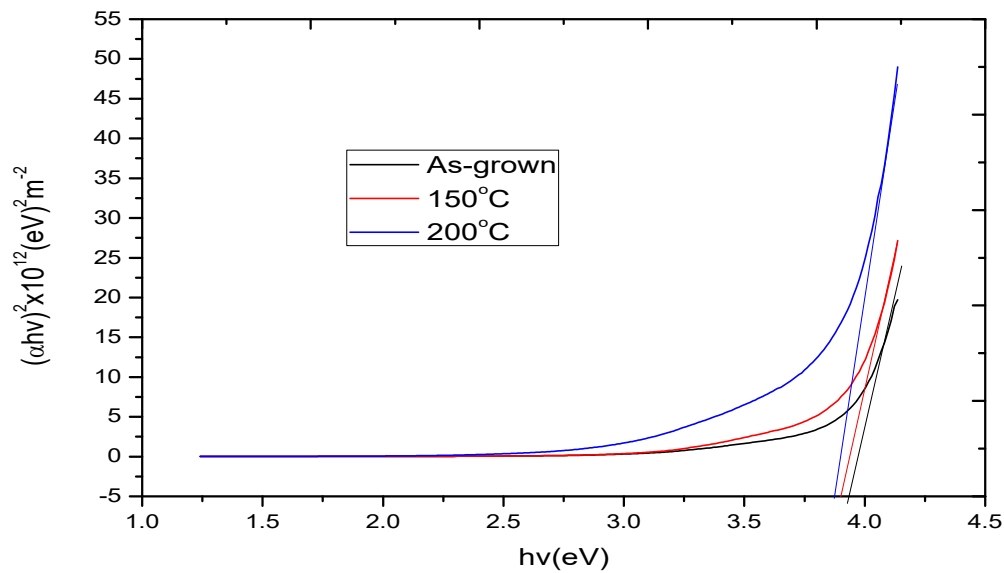


Fig.8: Plots of $(\alpha hv)^2$ versus photon energy

The high transparency in the visible region and wide direct band gap energy exhibited by our film samples make them ideal for use as window layer in heterojunction solar cells. The primary function of a window layer in a heterojunction is to form a junction with the absorber layer while admitting a maximum amount of light to the

junction region and the absorber layer [28]. The CIGS solar cells typically use a CdS window layer. However, there are great concern about the toxicity of Cd in this architecture [35] and so; several alternative window layers are currently being investigated to replace CdS. In our view, ZnS/Fe₂O₃ films deposited in this work stand high for possible incorporation in CIGS solar cell. Fig.9 is the plot of extinction coefficient against photon energy. The extinction coefficient generally increased with photon energy. It vary from 0.25 to 2.5 for as-grown layer, 0.25 to 3.0 for annealed at 150°C layer and 0.53-3.57 for annealed at 200°C. Our values of extinction coefficient are in agreement with the report of other authors [14]. However, it is lower that the report in the following reference [13, 36]. Fig.10 depicts the plot of refractive index versus photon energy. The refractive index has a maximum of 2.7 for all layers of the films with different minima values. The range of the refractive index values are in agreement with the report of other research groups [13, 14, 37-39].

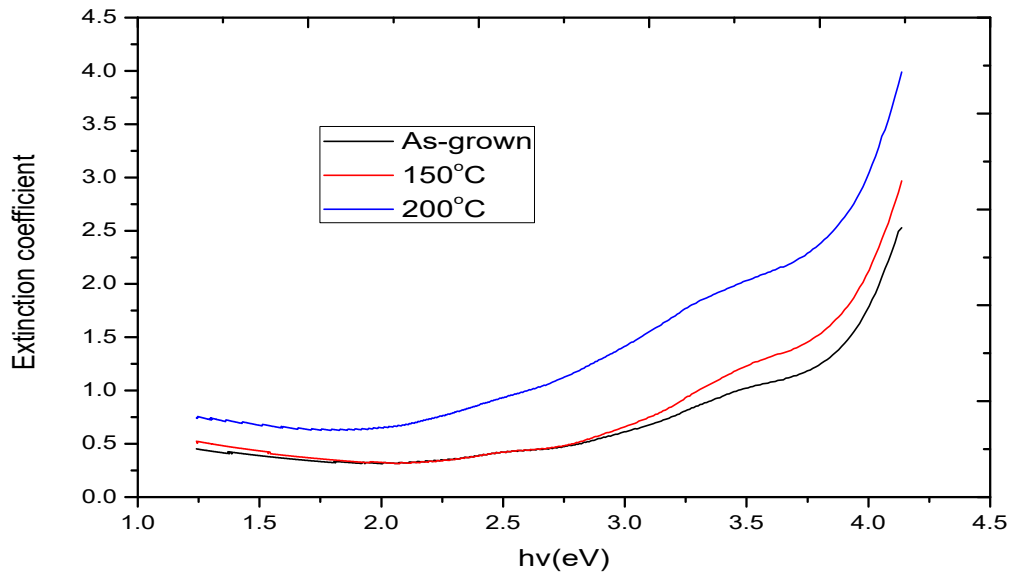


Fig.9: Plots of extinction coefficient versus photon energy

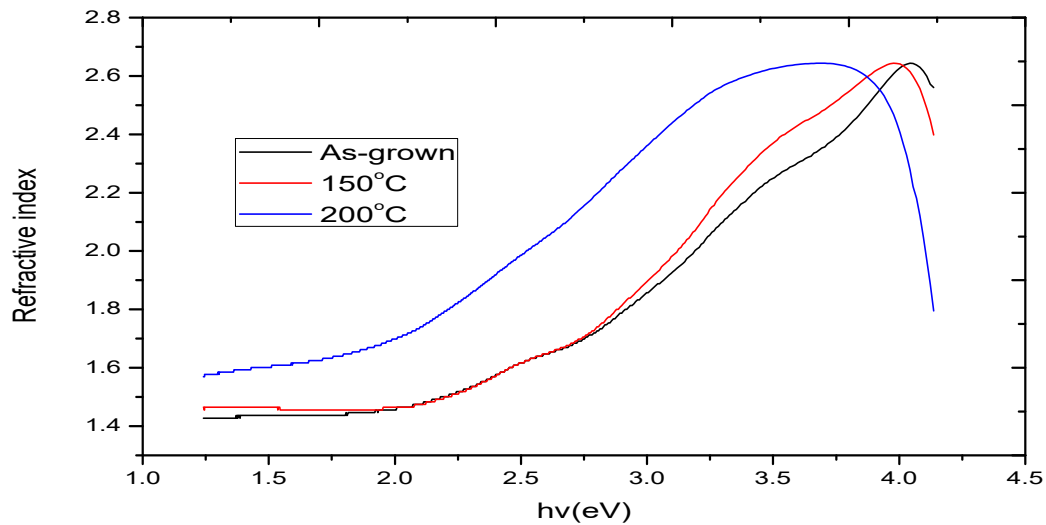


Fig.10: Plots of refractive index versus photon energy

Figures 11 and 12 are plots of real and imaginary parts of dielectric constant versus photon energy respectively. The real part of dielectric constant shows how much the speed of light slows down in the material, whereas the imaginary part of dielectric constant shows how a dielectric material absorbs energy from an electric field due to dipole motion. Both the real and imaginary parts of dielectric constants were computed using established equation in the literature [29].

$$\varepsilon_r = n^2 - k^2 \quad (1)$$

$$\varepsilon_i = 2ink \quad (2)$$

where ε_r and ε_i are the real and imaginary parts respectively of dielectric constant, n and k are refractive index and extinction coefficient respectively.

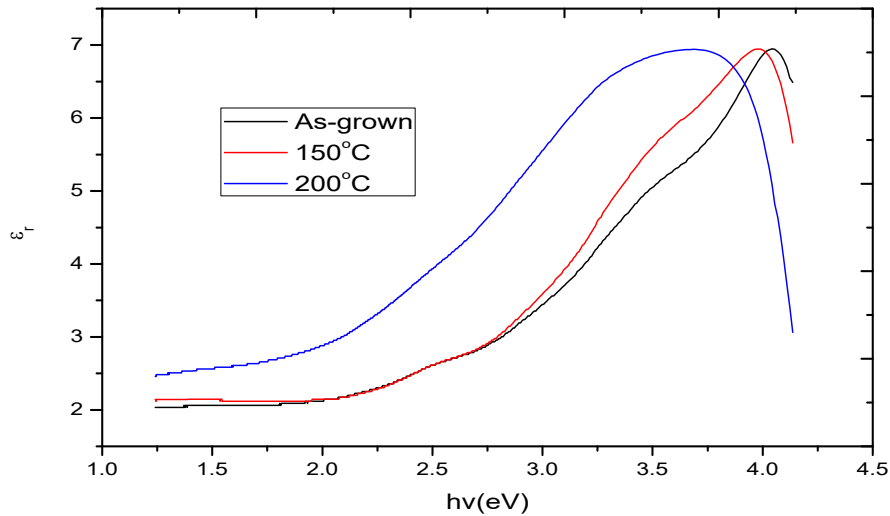


Fig.11: Plots of real dielectric constant versus photon energy

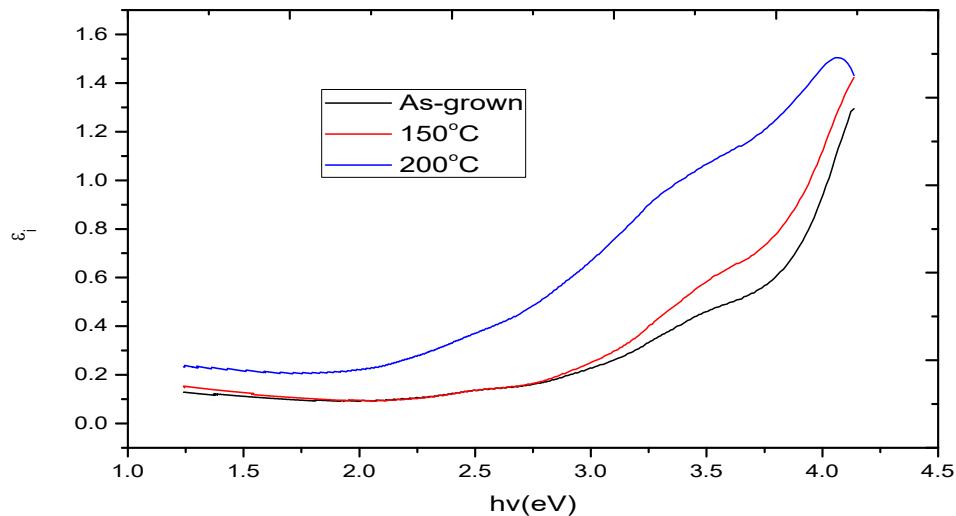


Fig.12: Plots of imaginary dielectric constant versus photon energy

A close observation of fig.11 shows that the real dielectric constant exhibited similar patterns with the refractive index plots. This may be due to the similarity in the mathematical relations used in computing both values of real dielectric and refractive index. Our values of real dielectric constant are in agreement with that of other authors [13, 36-38]. However, our values of imaginary dielectric constant are lower compared to the report of other authors in the literature [13, 36-38]. The values of the dielectric are within the range for use as layers for fabrication of devices with low capacitance requirements [13].

IV. CONCLUSION

The synthesis and characterization of ZnS/Fe₂O₃ thin films using chemical bath deposition technique was successfully carried out. The quantitative measurement of the elemental composition of the films showed that all the elements that make up the core-shell were present. The scanning electron micrographs of the films depicted homogeneity in particle distribution with post deposition temperature. The optical characterization was carried out using spectrophotometer. The optical and solid state parameters varied considerably with the parametric investigation involving post deposition temperature. In particular, the band gap energy exhibited a red shift, decreasing from 3.90eV to 3.85eV. The transmittance spectra of the films are in the range suitable as coating materials for the construction of poultry houses. The wide band gap of the films varied in the range suitable for solar cell fabrications, high frequency applications as well as optoelectronic applications.

REFERENCES

1. W.S. Seung, O.P. Hyun, S.M. Pawar, K. Jong-Ha, J. Hyeok, *Effect of complexing agent and annealing atmosphere on properties of nanocrystalline ZnS thin films*, *Journal of nanoscience and nanotechnology*, 10, 3686-3690 (2010).
2. L. I. Berger, *Semiconductor Materials (Physical Sciences References)*, CRC press, 1st edition, 186-187 (1996).
3. D. Su, H. S. Kim, W. S. Kim and G. Wang, "Synthesis of Tunable Porous Hematite (α -Fe₂O₃) for Gas Sensing and Lithium Storage in Lithium Ion Batteries," *Microporous and Mesoporous Materials*, 149, 36-45 (2012).
4. S.L. Mammah, F.E. Opara, F.B. Sigalo, S.C. Ezugwu and F.I. Ezema, *Annealing effect on the solid state and optical properties of α -Fe₂O₃ thin films deposited using the Aqueous Chemical Growth (ACG) methods*, 3, 793-801 (2012).
5. B. Avijit, "Pickard's Manual of Operative Dentistry," Oxford University Press Inc., New York, 89 (2011).
6. A.S. Teja, P. Y. Koh, "Synthesis, Properties, and Applications of Magnetic Iron Oxide Nanoparticles," *Progress in Crystal Growth and Characterization Materials*, 55, 22-45 (2009).
7. T. Marin, C. Nada, P. Matjaz, S. Zoran, M. S. Dragana and S. Vojstav, "Synthesis, Morphology, Microstructure and Magnetic Properties of Hematite Submicron Particles," *Journal of Alloys and Compounds*, 509, 7639-7644 (2011).
8. J. Singh, M. Srivastava, J. Dutta and P. K. Dutta, "Preparation & Properties of Hybrid Monodispersed Magnetic Fe₂O₃ Based Chitosan Nanocomposite Film for Industrial & Biomedical Application," *International Journal of Biological Macromolecules*, 48, 170-176 (2011).
9. M.A. Manal, H. H. Noor, I.M. Hanaa, H.M. Ghuson, A.A. Kadhim, and F.A. Ameer, *Investigation of optical properties of the PbS/CdS thin films by thermal Evaporation*, *Journal of Electron Devices*, 12 (2012) 761-766.
10. A.A. El Meh, S. Ershov, N. Britun, A. Richard, S. Kunstantinidis and R. Synders, *Combined optical emission and resonant absorption diagnostics of an Ar-O₂-Ce-reactive magnetron sputtering discharge*, *Spectrochimica Acta Part B*, 99-105 (2015).
11. K. Sergiy, R. Debnath, H.P. Youn, M.R. King, H. Jong-Yovh, B. Wen, A. Motayed and A.V. Davydov, *Faceting control ion core-shell GaN micropillars using selective epitaxy*, *APL Materials*, 2, 106104 (2014).
11. C. Augustine, M. N. Nnabuchi, F.N.C. Anyaegbunam, A.N. Nwachukwu, *Study of the effects of thermal annealing on some selected properties of Heterojunction PbS-NiO core-shell thin film*, *Digest Journal of Nanomaterials and Biostructures*, 12, 523-531 (2017).
12. M.N. Nnabuchi, C. Augustine, *Mn₃O₄/PbS thin films: preparation and effect of annealing temperature on some selected properties*, *Materials Research Express*, 5, 1-11 (2018).
13. C. Augustine, M.N. Nnabuchi, *Optical and solid state characterization of chemically deposited CuO/PbS double layer thin film*, *Materials Research Express*, 5, 1-11 (2018).
14. C. Augustine, M.N. Nnabuchi, F.N.C. Anyaegbunam, C.U. Uwa, *Annealing treatments and characterization of PbS-CdO core-shell thin film for solar energy applications*, *Chalcogenide Letters*, 14, 321-329 (2017).
15. C. Augustine, M.N. Nnabuchi, *Band gap Determination of Novel PbS-NiO-CdO Heterojunction thin film for possible Solar Energy Applications*, *Journal of Ovonic Research*, 13, 233-240 (2017).

16. C. Augustine, M.N. Nnabuchi, Band gap determination of chemically deposited lead sulphide based heterojunction thin films, *Journal of Non-Oxide Glasses*, 9, 85-98 (2017).
17. Y. Huang, Z. Zheng, Z. Ai, L. Zhang, X. Fan and Z. Zou, Core-shell microspherical solid solution photocatalysts directly from ultrasonic spray pyrolysis, *J.Phys.Chem*, 110, 19323-19328 (2006).
18. G. Taher, M.A. Al-Messiere, A.L. Al-Otaibi, Synthesis and characterization of ZnO/ZnS core-shell nanowires (2014). <https://doi/10.1155/2014/989632>.
19. K. Ahmadi, A.A. Ziabari, K. Mirabbaszadeh and A.A. Shal, Synthesis and characterization of ZnO/TiO₂ composite core-shell nanorod arrays by sol-gel method for organic solar cell applications, *Bull.Mater.Sci.*, 38, 617-623 (2017).
20. J. Schrier, D.O. Demchenko and L. Wang, Optical properties of ZnO/ZnS and ZnO/ZnTe heterostructures for photovoltaic applications, *Nano Letters*, 7, 2377-2382 (2007).
21. I.C. Ndukwe, "Growth and Characterization of Thin Chalcogenides films" PhD Thesis, University of Nigeria, Nsukka (1992).
22. P.E. Agbo, M.N. Nnabuchi and D.U. Onah, TiO₂/Fe₂O₃ core-shell thin film for photovoltaic application, *Journal of Ovonic Research*, 7, 29-35 (2011).
23. T. Soga, *Fundamental of solar cell nano-structured materials for solar energy conversion UK*, Elsevier, (2006) 3-4.
24. P.E. Agbo, M.N. Nnabuchi, D.U. Onah, TiO₂/Fe₂O₃ core-shell thin film for photovoltaic application, *Journal of Ovonic Research*, 7, 29-35 (2011).
25. V. S. Reddy, K. Das, A. Dhar, S. K. Ray, "The effect of substrate temperature on the properties of ITO thin films for OLED applications," *Semiconductor Science and Technology*, 21, 1747–1752 (2006).
26. F.I. Ezema, P.U. Asogwu, A.B.C. Ekweakor, P.E. Ugwoke and R.U. Osuji, *J.University of Chemical Technol. And Metall*, 42, 217 (2017).
27. P.N. Kalu, D.U. Onah, P.E. Agbo, C. Augustine, R.A. Chikwenze, F.N.C. Anyaegbunam and C.O.Dike, the influence of deposition time and annealing temperature on the optical properties of chemically deposited cerium oxide thin films, *Journal of Ovonic Research*, 14, 293-305 (2018).
28. R.A. Chikwenze, M.N. Nnabuchi, Properties of lead selenide films deposited by chemical bath method, *Chalcogenide Letters*, 7, 401-408 (2010).
29. W. Lou, X. Wang, M. Chen, W. Liu, J. Hao, *Nanotechnology*, 19 (2008) 225607.
30. J.P. Cheng, X.B. Zhang, and Z.Q. Luo, *Surface and coatings Tech*, 202, 4681 (2008).
31. D.S. Dhawale, A.M. More, S.S. Latthe, K.Y. Rajpure, C.D. Lokhande, *Applied Surface Science*, 254, 3269.
32. R. S. Vaidyanathan, *Interface*, 16, 2 (2007).
33. S.A. Cetin, L. Hikmet, *America Institute of Physics*. (2007).
34. K.L. Chopra, P.D. Paulson, V. Dutta, *Thin film solar cells: an overview*, *Prog Photovolt: Research Applications*, 12, 69-92.
35. C. Augustine, M. N. Nnabuchi, P. E. Agbo, F. N. C. Anyaegbunam, R. A. Chikwenze, C. N. Nwosu, P. N. Kalu, U. Uba, R. O. Okoro, S. O. Onyishi, Investigation of the effect of Lead ion (Pb²⁺) concentration on the optical and solid state properties of chemically deposited Mn₃O₄/Pb_{1-x}S heterojunction thin films, *Journal of Ovonic Research*, 14, 339-350 (2018).
36. P.E. Agbo, M.N. Nnabuchi, Core-Shell TiO₂/ZnO thin film: preparation, characterization and effect of temperature on some selected properties, *Chalcogenide Letters*, 8, 273-282 (2011).
37. P.E. Agbo, *Refractive Index and Dielectric Properties of TiO₂/CuO Core –Shell Thin Films*, *Chemistry and Materials Research*, 6, 42-45 (2014).
38. P.E. Agbo, *Effect of Thermal Annealing on Optical and Band gap of chemically deposited TiO₂/Fe₂O₃ Core/shell Oxide Thin Films*, *Advances in Applied Science Research*, 2, 393-399 (2011).